Hindawi
Advances in Polymer Technology
Volume 2023, Article ID 1893660, 17 pages
https://doi.org/10.1155/2023/1893660

Research Article

Biodegradable Composite of Gelatin Blend Microcrystalline Cellulose for Cd^{2+}, Pb^{2+}, and Cr^{3+} Adsorption from an Aqueous Solution

Marzia Sultana,[1] Md. Raju Ahmmed,[1] Md Inzamam Ul Hoque,[1] Tanvir Ebna Mohsen,[1] Atol Mondal,[1] Md. Hafezur Rahaman,[2] Moumita Yesmin,[1] Md. Shahedur Rahman,[3] and S. M. Nur Alam[1]

[1]*Department of Chemical Engineering, Jashore University of Science and Technology, Jashore 7408, Bangladesh*
[2]*Department of Applied Chemistry and Chemical Engineering, Islamic University, Kushtia 7003, Bangladesh*
[3]*Department of Genetic Engineering and Biotechnology, Jashore University of Science and Technology, Jashore 7408, Bangladesh*

Correspondence should be addressed to S. M. Nur Alam; smn.alam@just.edu.bd

Received 13 February 2023; Revised 9 June 2023; Accepted 12 June 2023; Published 29 June 2023

Academic Editor: Sikander Rafiq

Biodegradable and eco-friendly composite adsorbent was synthesized from modified jute fiber and gelatin and evaluated its efficacy in removing cadmium (Cd^{2+}), lead (Pb^{2+}), and chromium (Cr^{3+}) ions from an aqueous solution. The prepared sample was characterized using Fourier transform infrared spectroscopy, scanning electron microscopy, and energy dispersive X-ray analyses, which revealed that gelatin successfully intercalated into the microcrystalline cellulose matrix. In batch adsorption studies, the effects of pH, adsorbent dosage, initial metal ions concentration, and temperature on the removal of heavy metal ions were investigated. The adsorption capacity of the composite varied with changing parameters, and the maximum removal efficiency obtained for Cd^{2+}, Pb^{2+}, and Cr^{3+} was 95%, 88%, and 70%, respectively, at pH 6 with 60 ppm of each metal ions concentration and an adsorbent dosage of 1.0 g L^{-1}. Different functional groups in composite adsorbent facilitated heavy metal ions adsorption. Five error analysis methods were used to evaluate the fit the goodness of the data. The equilibrium adsorption and kinetic data were well-fitted with the Langmuir isotherm model and pseudo-second-order, respectively. Moreover, the thermodynamic study showed that the adsorption was spontaneous, chemisorption, and endothermic. Our work offers a sustainable and biodegradable composite synthesized from modified jute fiber and gelatin for multimetal ions removal from an aqueous, which is an eco-friendly alternative to conventional nonbiodegradable adsorbents with potential environmental risks.

1. Introduction

Heavy metals are potentially toxic if the concentrations surpass maximum permissible levels [1]. They come into the environment through natural and anthropogenic activities [2]. These metals are not degraded; they pose an even greater danger to organisms as they accumulate over time. Among the heavy metals, lead (Pb^{2+}), cadmium (Cd^{2+}), and chromium (Cr^{3+}) ions are widely used for various purposes [3]. The optimum concentration of Cd^{2+}, Pb^{2+}, and Cr^{3+} in the effluent may depend on the pollution control board standard value of the country or region where the wastewater is discharged. According to World Health Organization (WHO) [4], the permissible limits for Cd^{2+}, Pb^{2+}, and Cr^{3+} in clean water are 0.03, 0.01, and 0.003 mg L^{-1}, respectively. However, these values may vary depending on the environmental regulations and guidelines of different authorities. The concentration of Cd^{2+}, Pb^{2+}, and Cr^{3+} in industrial effluent in Bangladesh may vary depending on the type and source of the wastewater. However, one study [5] reported that the average concentration of Cd^{2+}, Pb^{2+}, and Cr^{3+} in industrial effluent samples collected from Dhaka city's river were 0.0041, 0.043, and 0.756 mg L^{-1}, respectively. These values exceeded the permissible limits set by the WHO. Therefore, it is important to treat the industrial effluent before releasing it into the environment to prevent water pollution and health risks.

Cd^{2+} is potentially toxic and can result in many chronic diseases like kidney, liver, renal failure, and cardiovascular disease of the human body, while Pb^{2+} has carcinogenic properties that harm respiratory, digestive, and immune systems; in children, it mostly disrupt the neurological system [6, 7]. On the other hand, above pH 6.0, chromium may exist in different oxidation states. The Cr^{3+} ions play an important role in living organisms by maintaining cholesterol, triglycerides, and glucose levels. However, under certain conditions, Cr^{3+} is easily oxidized to Cr^{6+} and causes several environmental problems for its high mobility and solubility. It can also harm the kidney, liver, skin, and respiratory systems, leading to dermatitis, lung cancer, and nasal septum perforation [8]. Therefore, elimination of these heavy metal ions from industrial effluent is urgently required.

Different techniques, such as adsorption [9], ion exchange [10], membrane filtration [11], chemical precipitation [12], reverse osmosis [3], and solvent extraction [13] have been employed to eliminate heavy metal ions from the industrial effluent. Adsorption is an economical and cost-effective process of removing heavy metals. This technique is easy to operate and almost removes heavy metal ions entirely from an aqueous solution [14]. Various materials have been used, including clay, lignocellulosic materials, agricultural waste, zeolite, sewage waste, fly ash, and activated carbon, for treating wastewater containing heavy metal ions [2]. Activated carbon is the most well-known substance for removing metal ions from aqueous solution. However, practical applications are limited due to their high price and regeneration cost [14]. In contrast, adsorbent synthesis from plant origin is environmentally friendly and very effective for eliminating heavy metal ions from industrial effluents. In addition, these adsorbents are readily available, inexpensive, and easy to synthesize [15]. Cellulose, a naturally occurring polymer, is an environmentally benign and biodegradable adsorbent. It can be tailored into different functional groups or composites using different reagents due to containing many hydroxyl groups [16]. Modified cellulose exhibited higher adsorption capacity than unmodified cellulose toward heavy metal ions. For example, cellulose modified by different functionalized group showed superior adsorption capacity toward inorganic toxic contaminants than those of untreated cellulose [17]. Composite made from cellulose and dibenzo-18-crown six showed superior adsorption capacity toward heavy metal ions than those of untreated cellulose [18]. Microcrystalline cellulose (MCC) derived from jute fiber is very effective in removing heavy metal ions from an aqueous solution [15].

Gelatin is a naturally occurring high molecular weight polypeptide that may be found in various animal sources, including the skin of pigs, cattle, and fish. It is water soluble, nontoxic, and biodegradable [19]. It is frequently employed in the food sector to improve the texture of meals, biomedical applications, and controlled drug release systems in therapeutic procedures [20]. Gelatin is a very effective adsorbent due to the polymorphism structure of its functional amino acid group and carboxyl acid groups [21]. However, the combination effects of gelatin and MCC as an adsorbent were not reported anywhere.

The innovation of this work lies in the development of a biodegradable composite adsorbent made from gelatin and modified cellulose that effectively removes toxic heavy metal ions from industrial effluent. The use of a composite material synthesized from plant-derived cellulose and naturally occurring gelatin is environmentally friendly, and easily synthesized. The study also explores the effectiveness of this adsorbent in removing Cd^{2+}, Pb^{2+}, and Cr^{3+} ions from an aqueous solution and examines the effects of different parameters such as pH, adsorbent dosage, initial metal ions concentration, and temperature on the removal efficiency. The findings of this study can contribute to the development of sustainable and eco-friendly solutions for heavy metal ion removal in industries and help in mitigating the adverse effects of heavy metal pollution on the environment and human health.

In this study, we investigated the adsorption performance of the MCC–gelatin composite for the simultaneous removal of Cd^{2+}, Pb^{2+}, and Cr^{3+} ions from aqueous solutions under different conditions. We also studied the adsorption mechanism and thermodynamics of the process using various models and equations.

2. Experimental

2.1. Materials and Reagents. Corchorus olitorius (Tossa Jute), collected from the local market of Jashore Sadar, Bangladesh, was used as a raw material for MCC source. A suitable portion of 25 cm fiber was taken. Analytical-grade chemicals were used in this experiment. Glassware used in the tests was cleaned with a 3% HNO_3 solution before being rinsed several times with distilled water. $CdSO_4$, $Pb(NO_3)_2$, and $Cr(NO_3)_3$ salts were used to make 1,000 ppm concentrated stock solutions of Cd^{2+}, Pb^{2+}, and Cr^{3+} ions, respectively. These metal solutions were further diluted with distilled water to prepare various concentrated solutions that are required for the experiments.

2.2. Preparation of α-Cellulose. The procedure for the preparation of MCC adsorbent is based on the previous literature [15]. Cleaned and dried raw jute fiber was cut into small pieces around 2-3 cm. Jute fiber was bleached using a 7.0 g L^{-1} concentrated sodium chlorite ($NaClO_2$) solution, and pH 4.0 was adjusted by adding 2 M CH_3COOH solution. Bleaching was carried out at a temperature of 85–90°C for 90 min using 80 ml solution for each gram of fiber and successfully removed the lignin from the fiber. After the bleaching process, the fiber was thoroughly cleaned with distilled water before drying at 80°C. Then, 17.5% NaOH (fiber: NaOH ratio 1 g: 25 mL) was used to treat the resulting fiber at room temperature to eliminate both β and γ cellulose. After that, the α-cellulose was washed with 2% acetic acid and water alternatively and dried at 60°C [22].

2.3. Preparation of Microcrystalline Cellulose (MCC). Two gram of α-cellulose was washed with distilled water to eliminate any adhering or water-soluble particles, dried at 85°C, and then treated with 20 mL of H_2SO_4 (0.1 N) with continuous shaking for 30 min. The pH of the fiber was brought to neutral by rinsing it with distilled water. Finally, the residue

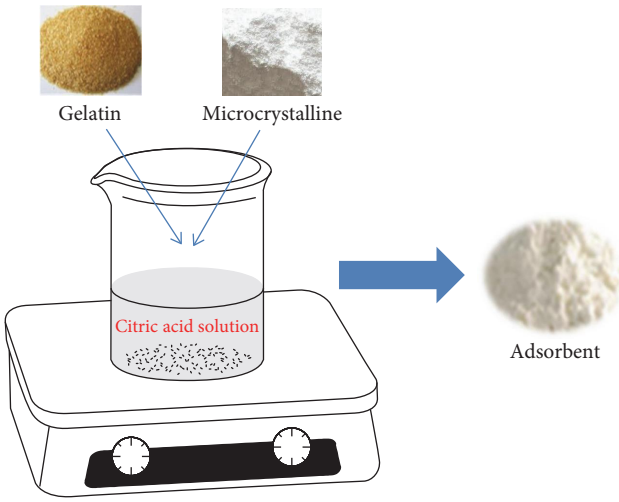

Figure 1: Preparation method of composite adsorbent.

was dried at 60°C and ground with mortar and pestle until it turned into a fine powder.

2.4. Synthesized of Gelatin Blend Microcrystalline Cellulose Composite. An amount of 10 wt% gelatin blend-modified cellulose was prepared by pouring 0.2 g of gelatin into 1 wt% citric acid solution and stirring for 3 hr to produce a gel-like solution as shown in Figure 1 [23]. Then, 2 g of MCC powder was added to the gel-like solution and stirred at 40°C temperature for 3 hr. The residue was dried at 60°C and ground with mortar and pestle until it turned into a fine powder.

2.5. Characterization. Different techniques were used to characterize the synthesized gelatin blend microcrystalline composite adsorbent. First, the shape, size, and morphology of the adsorbent were examined using scanning electron microscopy (SEM) on a ZEISS Sigma 300 model with an accelerating voltage of 5 kV and a working distance of 7.9–8.0 nm. After that, the elemental compositions of the samples were determined using a Bruker X Flash 630 energy dispersive X-ray (EDX) microanalysis system coupled to the SEM. Finally, Nicolet iS20 attenuated total reflection Fourier transform infrared spectroscopy (Thermo Scientific) was used to generate FTIR spectra using the KBr tablet technique.

2.6. Batch Adsorption Experiments. Batch adsorption of Cd^{2+}, Pb^{2+}, and Cr^{3+} ions was carried out under various conditions, including pH, temperature, the dose of the adsorbent, starting metal ion concentrations, and contact times. The influence of pH on metal ions adsorption was evaluated by changing the pH from 2 to 6 using 0.1 g of adsorbent in 100 mL of 60 ppm of each metal ion concentrated solution. The initial metal ions concentration effect on adsorption was carried out in varying from 10 to 100 ppm at pH 6 using 1 g L^{-1} adsorbent. An adsorbent dosage (0.5–2.5 g L^{-1}) variation was assessed at pH 6 using 60 ppm of each metal ion concentrated solution. In addition, to conduct contact time tests, 0.1 g of adsorbent

Table 1: Equations of the error function used in the study.

Equation	Reference
$\text{HYBRID} = \frac{100}{(N-P)}\sum_{i=1}^{n}\frac{(q_{e,exp}-q_{e,cal})^2}{q_{e,exp}}$	[25]
$\text{MPSD} = 100\sqrt{\left(\frac{1}{N-P}\right)\sum_{i=1}^{n}\frac{(q_{e,exp}-q_{e,cal})^2}{q_{e,exp}}}$	[26]
$\chi^2 = \sum_{i=1}^{n}\frac{(q_{e,exp}-q_{e,cal})^2}{q_{e,cal}}$	[27]
$\text{RMSE} = \sqrt{\frac{1}{N-2}\sum_{i=1}^{n}(q_{e,exp}-q_{e,cal})^2}$	[11]
$\text{EABS} = \sum_{i=1}^{n}\lvert q_{e,exp}-q_{e,cal}\rvert$	[28]

was employed in 100 mL of 60 ppm metal ions concentration solution at pH 6 for 80 min. Three different temperatures 25, 35, and 45°C, were employed to investigate the thermodynamics studies. The atomic absorption spectrophotometer (AAS) was used to measure the metal ions concentration in the filtrate solution. The following Equation (1) determined the removal percentages of Cd^{2+}, Pb^{2+}, and Cr^{3+} ions in the adsorbent.

$$\text{Metal ion removal}\,(\%) = \frac{(C_o - C_e)}{C_o} \times 100\%, \tag{1}$$

where C_o (mg L^{-1}) and C_e (mg L^{-1}) are the initial and the equilibrium metal ion concentration in the solution.

The following Equation (2) was used to calculate the adsorption capacity: the quantity of metal ions adsorbed per unit mass of gelatin blend MCC composite adsorbent (mg g^{-1}).

$$q_e = \frac{[(C_o - C_e) \times V]}{M}, \tag{2}$$

where q_e (mg g^{-1}) and C_e (mg L^{-1}) are the adsorbate amount and metal ions concentration, respectively, at equilibrium. C_o (mg L^{-1}) is the initial metal ions concentration, M (g) is the used composite adsorbent amount, and V (L) is the solution volume [24].

2.7. Error Function Analysis. Apart from the regression coefficient (R^2), the suitability of the experimental results is also assessed by error function. Five error functions given in Table 1 including, hybrid functional error (HYBRID), Marquardt's percent standard deviation (MPSD), nonlinear chi-square test (χ^2), residual root-mean-square error (RMSE), and sum of absolute error (EABS) were calculated to assess the best fit of the modeled equation to the experimental data.

Where $q_{e,\,exp}$ (mg g^{-1}) is the batch experiment value and $q_{e,\,cal}$ (mg g^{-1}) is the corresponding calculated value from the isotherm for $q_{e,\,exp}$ (mg g^{-1}). N is the number of observations in the experimental isotherm, and P is the number of parameters.

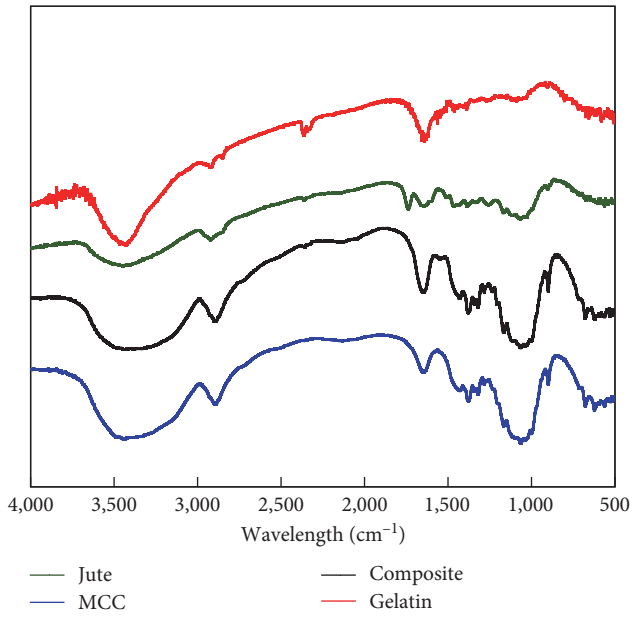

Figure 2: FTIR spectra of jute, MCC, composite, and gelatin.

Table 2: Peaks position of different functional groups band absorption for microcrystalline cellulose, gelatin, and biodegradable composite from their FTIR spectra [15, 33].

Accounted Bond for the Absorption (cm^{-1})	Microcrystalline cellulose (MCC) (cm^{-1})	Gelatin (cm^{-1})	Composite (cm^{-1})
(3,600–2,500) –OH stretching	3,335	3,257	3,298
(3,100–2,900) –CH stretching (Asym)	2,891	–	–
(1,780–1,650) –C = O stretching	–	1,620	–
(1,390–1,365) –C–H def bending	1,320	–	–
(1,250–1,050) –C–O– stretching	1,157	–	–
(1,200–1,020) –C–O–C bending	1,034	–	1,023
β–Glycosidic linkage	894	–	884
(1,680–1,200) Amide linkage	–	1,262	1,278

3. Results and Discussion

3.1. Characterization of Adsorbent

3.1.1. FTIR Analysis of Adsorbent. The FTIR spectra of jute, MCC, composite, and gelatin samples are shown in Figure 2. Stretching vibration of –OH groups was associated with the band at 3,453 cm^{-1}, while C–H stretching was associated with the band at 2,924 cm^{-1} [29]. The jute fiber showed a peak at 1,735 cm^{-1} for the carbonyl group, originating from acetyl ester in hemicellulose and aldehyde carbonyl in lignin [30]. However, the characteristic peaks of carbonyl group were not observed for the MCC. These results indicate that the treatment for α-cellulose extraction and modification successfully removed hemicellulose and lignin from the raw jute fiber. In addition, different peaks including C–OH, C–O–C, and C–C bonds absorption were more exposed on the surface due to acid hydrolysis of the amorphous cellulose, increasing stretching absorbency with a lower wavenumber and providing more support for jute fiber modification [15].

FTIR spectra (Figure 2) revealed the characteristic functional groups of both cellulose and gelatin present in the gelatin blend MCC composite. Table 2 gives the different functional group peaks position of these FTIR spectra. The peak of –OH group stretching vibration in MCC was around 3,448 cm^{-1} and moved in the direction of the lower wave number for the gelatin blend microcrystalline composite at 3,444 cm^{-1}. This change demonstrated that amine groups in gelatin and –OH groups in cellulose were interacted [31]. The peaks for carbonyl group of the composite were shifted to a higher frequency from 1,637 to 1,647 cm^{-1}. The vibrational peak intensity of the amide-II band in the composite adsorbent was shifted to a higher wave number at 1,278 cm^{-1} as gelatin interacted with the cellulose component through a

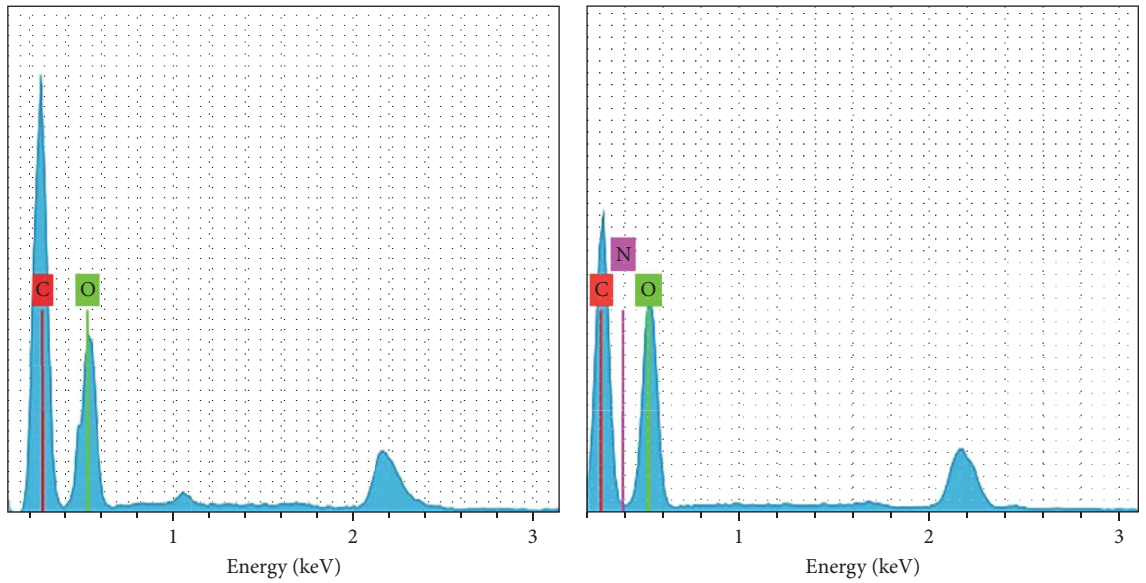

Figure 3: EDX mapping of (a) microcrystalline cellulose and (b) composite adsorbent.

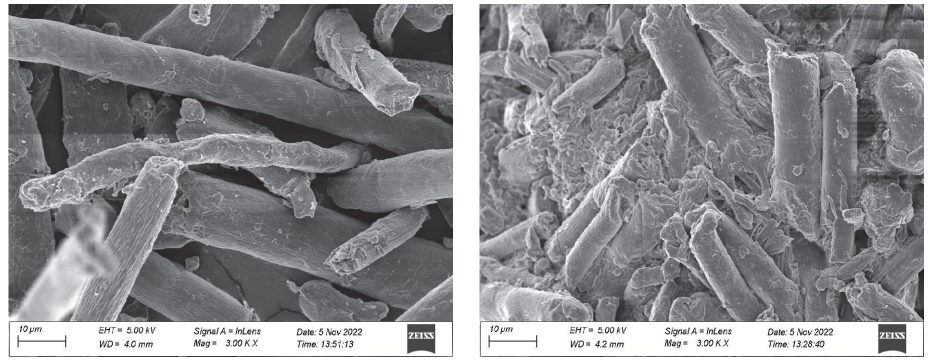

Figure 4: SEM images of (a) microcrystalline cellulose and (b) composite adsorbent.

new hydrogen bond formation. This FTIR spectrum revealed that the composite was formed by interacting the functional group of gelatin with the –OH group of treated cellulose [32].

3.1.2. Compositional Analysis. The nitrogen functional groups introduced on composite were confirmed by EDX analysis as shown in Figure 3. MCC extracted from jute fiber was nitrogen free while composite showed nitrogen element after interaction with gelatin. The elemental ratios of carbon and oxygen for MCC were 59.27% and 40.73%, whereas, carbon, oxygen, and nitrogen for prepared composite adsorbent ratio were 43.41%, 47.31%, and 9.29%, respectively.

3.1.3. Scanning Electron Microscopy Analysis. The morphology of the composite was examined by SEM to analyze the interaction between MCC and gelatin. Figure 4 shows that the lengthy chain of MCC was broken down into a smaller length and diameter in the composite during synthesis. The mean lengths and diameters of the composite fiber were 19.67 ± 7.86 and $6.07 \pm 2.27\ \mu$m, respectively. The increased cracking and irregularity of the cellulose structure demonstrated the modification of cellulose during composite formation.

The microstructure of MCC and composite was compared and analyzed in Figure 5. The surfaces of the MCC was relatively uniform, smooth, and flat, while the aggregate and relatively higher pores surface were observed for the composite. The figures show that the gelatin dispersed uniformly over the MCC surface, indicating high interaction between gelatin and MCC molecules. The addition of gelatin increased voids on the MCC surface was the most obvious because the two substances arranged their molecule differently during the composite formation process [33].

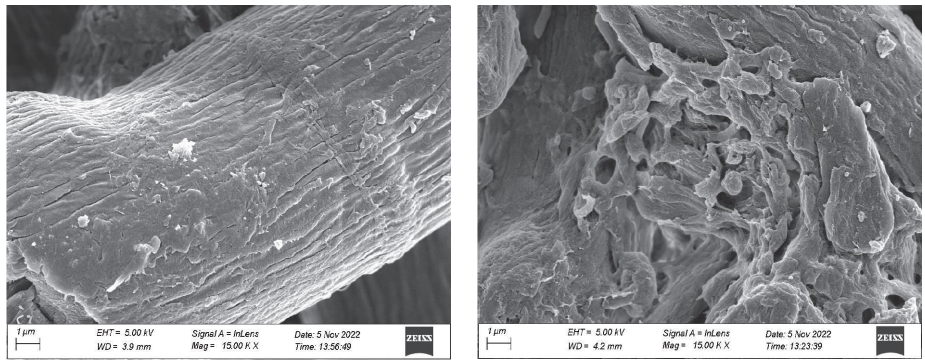

(a) (b)

FIGURE 5: Microstructure of (a) microcrystalline cellulose and (b) composite.

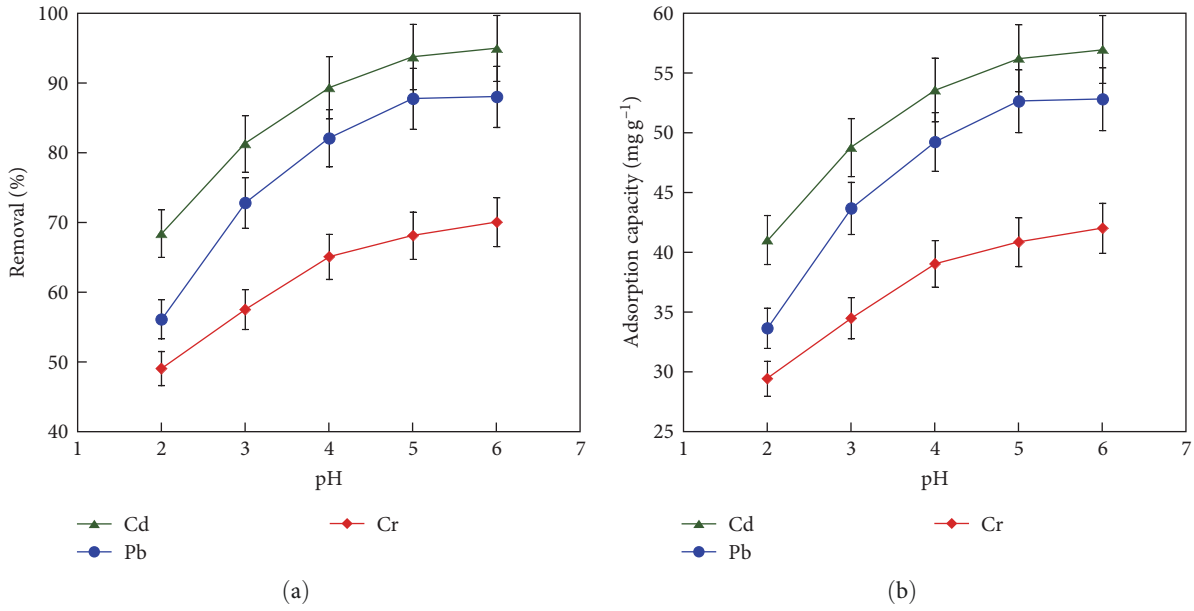

(a) (b)

FIGURE 6: Effect of pH on (a) removal percentage and (b) adsorption capacity of Cd^{2+}, Pb^{2+}, and Cr^{3+}, by composite adsorbent ($T = 298$ K, $t = 60$ min, dose = 1 g L^{-1}, and 60 ppm concentration).

3.2. Batch Adsorption Experiments

3.2.1. Effect of pH on the Metal Ions Adsorption. The pH of the solution greatly influences heavy metal adsorption to the adsorbent surface. The current study investigated the impacts of pH on Cd^{2+}, Pb^{2+}, and Cr^{3+} ions adsorption at 25°C. Heavy metals begin to precipitate in an alkaline medium as metal oxides or hydroxides; therefore, the experiment was carried out under acidic conditions (pH 2–6) using 0.1 g of adsorbent in 100 mL of a solution containing 60 ppm of each metal ion concentration [15]. Metal ions removal percentages increased with increasing solution pH from 2 to 6, as shown in Figure 6. The adsorption capacity of the composite was low at pH 2 because H^+ ions competed with metal ions for adsorption. In addition, the adsorbent's surface becomes the positive charge in an acidic medium, causing the metal ions and the adsorbent to repel each other [34].

Gelatin is an ampholytic polyelectrolyte with an isoelectric point around 4.8 [35]. The number of protons decreased with increasing pH value, minimizing the competition between metal and hydrogen ions. In addition, the adsorbent provided more active sites for the metal ion's adsorption due to the increased negatively charged carboxylic groups, thus improving the composite adsorption capacity. The removal efficiency of Cd^{2+}, Pb^{2+}, and Cr^{3+} ions were 95.11%, 88.13%, and 70.07%, respectively, with corresponding adsorption capacity 57.07, 52.88, and 42.04 mg at pH 6, which are similar to the previously reported [15].

3.2.2. Effect of Adsorbent Doses on the Metal Ions Adsorption. Figure 7 depicts the effects of various adsorbent doses (0.5, 1.0, 1.5, 2.0, and 2.5 g L^{-1}) on the adsorption of Cd^{2+}, Pb^{2+}, and Cr^{3+}. The experiments were conducted at pH 6 with 60 ppm of each metal ion concentration at 25°C. As more active sites were available for metal ions adsorption, the

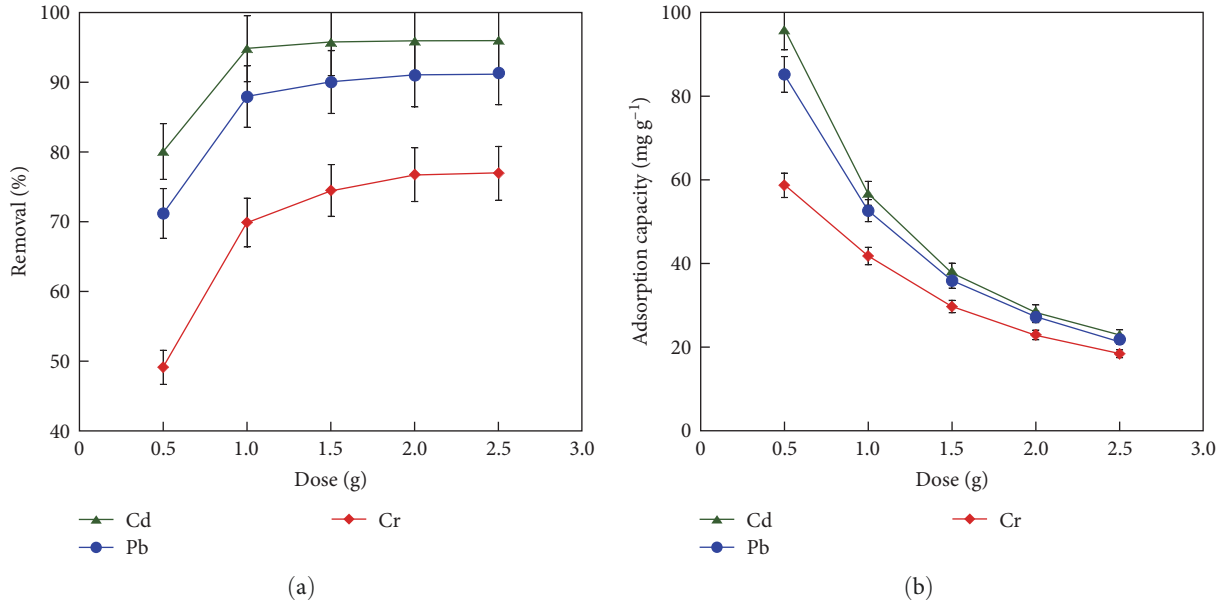

FIGURE 7: Effect of the adsorbent dosage on (a) removal percentage and (b) adsorption capacity of Cd^{2+}, Pb^{2+}, and Cr^{3+} by composite ($T = 298$ K, metal ions concentration = 60 ppm, pH-6, and $t = 60$ min).

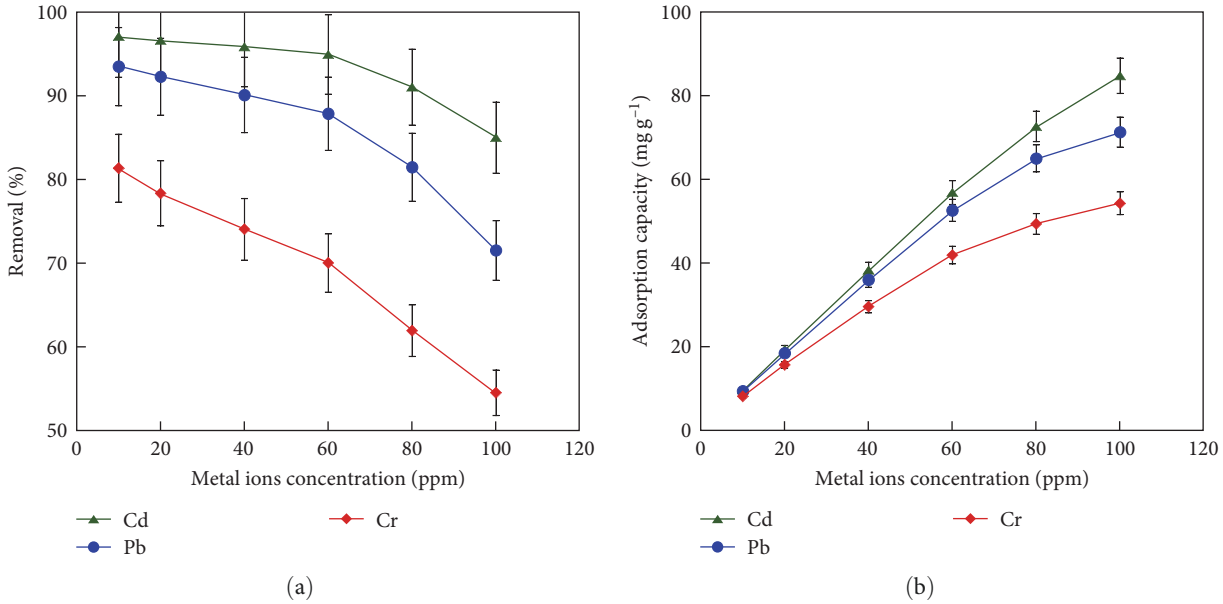

FIGURE 8: Effect of metal ion concentration on (a) removal percentage and (b) adsorption capacity of by composite ($T = 298$ K, $t = 60$ min, dosage = 1 g L^{-1}, and pH = 6).

removal percentage of Cd^{2+}, Pb^{2+}, and Cr^{3+} ions increased with increasing adsorbent dosage [18]. However, adsorption capacity falls with increasing the adsorbent dosage because of decreasing metal ions to active sites ratio. The rate of removal percentage decreased when adsorbent dosage above 1 g L^{-1} and therefore, adsorbent dose with 1 g L^{-1} was considered as optimum for 60 ppm metal ions concentrated solution [36]. The removal efficiency of Cd^{2+}, Pd^{2+}, and Cr^{3+}, was 95.06%, 88.17%, and 70.02% at pH 6.0 with corresponding adsorption capacity 57.04, 52.90, and 42.01 ppm, respectively.

3.2.3. Effect of Concentration on the Metal Ions Adsorption. Figure 8 shows the effect of initial concentration on Cd^{2+}, Pb^{2+}, and Cr^{3+} ions removal percentage and adsorption capacity. The initial metal ions concentration was changed from 10 to 100 ppm for all metal ions, while the other parameters were kept unchanged (metal solution pH: 6 and adsorbent dose: 1 g L^{-1}). The adsorption capacity increased linearly with the increasing initial concentration of each metal ion up to 60 ppm then dropped the adsorption capacity rate on further metal ions concentration. The removal efficiency of Cd^{2+}, Pb^{2+}, and Cr^{3+} ions at 60 ppm

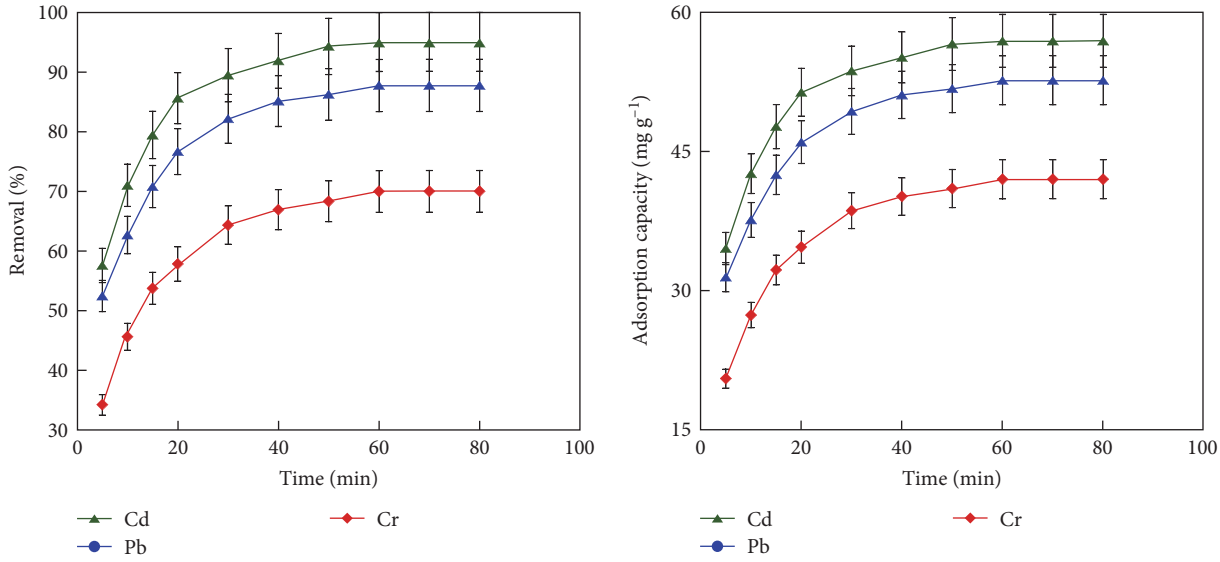

FIGURE 9: Effect of contact time on the (a) removal percentage and (b) adsorption capacity of Cd^{2+}, Pb^{2+}, and Cr^{3+} by composite ($T = 298$ K; dosage = 1 g L^{-1}; pH = 6).

concentration was 95.05%, 87.95%, and 70.03%, respectively. The highest removal percentage of each metal ion was observed at low concentrations because there were fewer metal ions in the active sites on the adsorbent. However, the comparative active sites were decreased for adsorption with increasing the initial metal ions concentration, which dropped the removal percentage [15].

3.2.4. Effect of Contact Time on the Metal Ions Adsorption. In adsorption studies, the time takes for metal ions adsorption to achieve equilibrium is crucial because of providing an idea about the adsorption mechanism. Figure 9 shows the Cd^{2+}, Pb^{2+}, and Cr^{3+} removal percentage and adsorption capacity with a contact time of 80 min. The equilibrium state almost reached 60 min, and the removal efficiency of Cd^{2+}, Pb^{2+}, and Cr^{3+} was 95.03%, 87.90%, and 70.10%, with the corresponding adsorption capacity 57.02, 52.74, and 42.06 ppm, respectively. The adsorption rate of the metal ions was high at first and reduced with increasing contact duration. The enhanced availability of active sites on the adsorbents is related to the rapid adsorption in the early phases. Adsorption occurs quickly and is governed by the diffusion process from the bulk to the surface of adsorbent [37]. The adsorption rate dropped with increasing contact duration as the active sites were used up and eventually achieved equilibrium; because there were fewer available adsorption sites, sorption was perhaps an attachment-regulated process.

3.2.5. Adsorption Isotherms. An adsorption isotherm is important for understanding the dynamic interaction between metal ions and composite adsorbent. The adsorption isotherms were assessed using the Langmuir, Freundlich, Tempkin, and Dubinin–Radushkevich (D–R) isotherm models. Equations (3–6) provide the linearized formula for all the above isotherm models. The correlation coefficients (R^2) equal to ~1 were used to index the extent of agreement between the experimental data and the isotherm model for all the isotherms.

The Langmuir model assumes that a monolayer is formed across the sorption sites during adsorption, while the Freundlich isotherm is employed for heterogeneous surface energy change of the adsorbent [11]. Temkin model describes the adsorbate/adsorbent interaction, while D–R model suggests the types of adsorption [4].

$$\frac{C_e}{q_e} = \frac{1}{q_m} C_e + \frac{1}{q_m K_L}, \tag{3}$$

$$\log q_e = \log K_F + \frac{1}{n} \log C_e, \tag{4}$$

$$q_e = B_T \ln A_T + B_T \ln C_e, \tag{5}$$

$$\log q_e = \log q_D + B_D [\ln (1 + 1/C_e)]^2, \tag{6}$$

$$E_D = \frac{1}{\sqrt{2B_D}}, \tag{7}$$

where C_e (mg L^{-1}) is the equilibrium concentration of Cd^{2+}, Pb^{2+}, and Cr^{3+} ions in aqueous solution and q_e (mg g^{-1}) is the amount of metal ions adsorbed at equilibrium state. q_m (mg g^{-1}) is the maximum adsorption capacity of Cd^{2+}, Pb^{2+}, and Cr^{3+} ions. K_L and K_F (L mg^{-1}) are the constants for the Langmuir and Freundlich isotherm models, respectively. A_T and q_d are the equilibrium binding constant (L min^{-1}) and the degree of sorbate sorption by the sorbent surface of Tempkin and D–R models, respectively.

Figure 10 depicts Langmuir, Freundlich, Tempkin, and D–R models for removing Cd^{2+}, Pb^{2+}, and Cr^{3+} at pH 6 by the composite adsorbent. Table 3 provides the adsorption isotherm values generated from all isotherms model. The

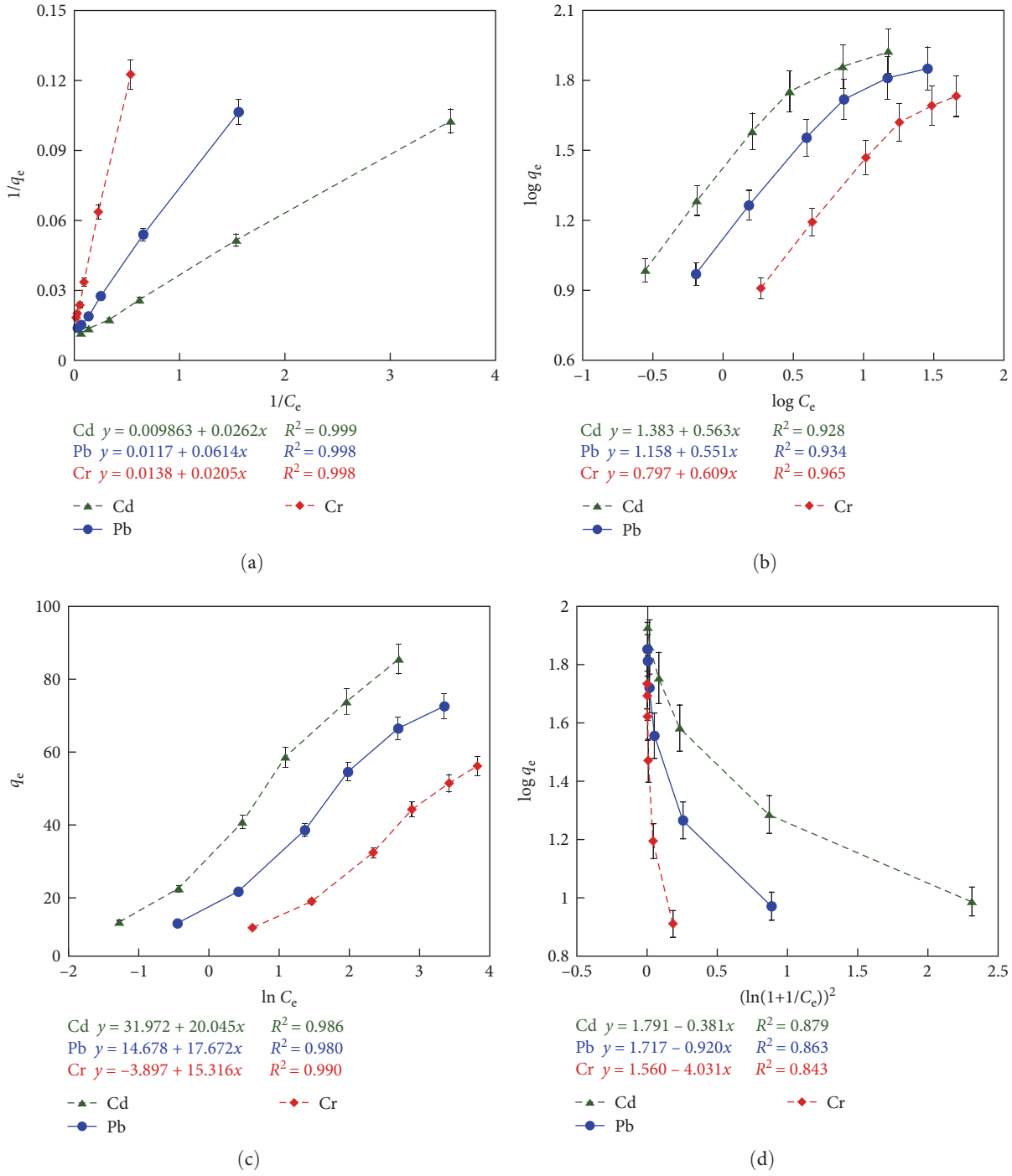

FIGURE 10: Isotherm plots of metal ions adsorption; (a) Langmuir model, (b) Freundlich model, (c) Tempkin model, and (d) Dubinin–Radushkevich model ($T = 298$ K; $t = 60$ min; dosage = 1 g L^{-1}, and pH = 6).

q_m and K_L are calculated from the intercepts and slopes of the straight lines on the $1/q_e$ versus $1/C_e$ plot. The graph of the Langmuir model is better suited to reflect the experimental data compare to among all isotherm models, as seen in the highest regression coefficient R^2 for all metal ions adsorption. These results indicate the chemisorption mechanism and support the homogeneous adsorption of Pb^{2+}, Cd^{2+}, and Cr^{3+} ions onto the composite adsorbent. Furthermore, since the uptake values are consistent with the Langmuir model, the monolayer and homogenous adsorption was considered for these metal ions. Thus, the maximum adsorption capacities of Pb^{2+}, Cd^{2+}, and Cr^{3+} calculated by the Langmuir model were 85.485, 101.420, and 72.213 mg g^{-1}, respectively. The parameters K_f and n in the Freundlich isotherm stand for surface dissimilarity and adsorption efficiency, respectively. Slope and intercept in log q_e versus log C_e plot provide $1/n$ and log K_f value, respectively. All analyzed metal ions adsorption had n values of more than 1, suggesting that

Table 3: Adsorption isotherm data for Cd^{2+}, Pb^{2+}, and Cr^{3+} onto the composite adsorbent.

Adsorption model	Parameters	Cd^{2+}	Pb^{2+}	Cr^{3+}
Langmuir model	q_{max} (mg g^{-1})	101.420	85.485	72.213
	K_L (L mg^{-1})	0.376	0.191	0.068
	R_L	0.117	0.208	0.425
	R^2	0.999	0.998	0.998
Freundlich model	K_f (L mg^{-1})	24.378	14.388	6.281
	1/n (L g^{-1})	0.553	0.551	0.609
	n (g L^{-1})	1.808	1.815	1.642
	R^2	0.928	0.934	0.965
Tempkin model	A_T (L mg^{-1})	4.928	2.295	0.548
	B_t (kJ mol^{-1})	20.045	17.672	18.647
	R^2	0.986	0.980	0.990
D–R model	q_D (mg g^{-1})	69.695	58.776	48.764
	E_D (kJ mol^{-1})	0.896	0.483	0.217
	B_D	0.622	2.145	10.57
	R^2	0.879	0.863	0.843

the adsorbent surface is heterogeneous and easy to separate ions from the solution, indicating a favorable adsorption process [38].

The data fitted to the linear equation in Tempkin's isotherm model, explain the adsorbent–adsorbate interactions. The equilibrium binding constant ($L\,min^{-1}$) corresponding to the highest binding energy is denoted as A_T in Tempkin's equation [39]. Tempkin's isotherm was validated by the graphs of q_e versus $\ln C_e$. The physicochemical properties of the adsorption process were explained by the D–R isotherm model. This model was used to calculate the apparent energy of adsorption and the theoretical saturation capacity.

As given in Table 3, the correlation coefficients of three metal ions adsorption onto composite adsorbent for the D–R isotherm model are less than $R^2 \leq 0.900$, which indicates a very poor correlation [11]. Therefore, the D–R isotherm is not a suitable model for the adsorption isotherm of Cd^{2+}, Pb^{2+}, and Cr^{3+} ions onto the adsorbent throughout the adsorption period.

3.2.6. Adsorption Kinetics. The absorption kinetics was investigated from data of different time adsorption. The experimental results were analyzed using pseudo-first-order (PFO) [40] and pseudo-second-order (PSO) [11] kinetic models. Equations (8) and (9) present the PFO and PSO models.

$$\log(q_e - q_t) = \log q_e - \frac{k_1 t}{2.203}, \tag{8}$$

$$\frac{t}{q_t} = \frac{1}{k_2 q_e^2} + \frac{1}{q_e} t, \tag{9}$$

where t (min) is the reaction time. k_1 (min^{-1}), and k_2 (g mg^{-1} min^{-1}) are the adsorption rate constants for PFO and PSO, respectively. The adsorption at the equilibrium and time t is denoted by q_e, and q_t for all metal ions adsorption. The slopes of the $\log(q_e - q_t)$ versus t and t/q_t versus t are used to determine the rate constants for the PFO and PSO kinetic models, respectively.

Figure 11 shows the PFO and PSO kinetic models data for Cd^{2+}, Pb^{2+}, and Cr^{3+} ions adsorption. The kinetic parameters calculated based on the above equations are given in Table 4. The experimental data fit better with the PSO equation ($R^2 > 0.99$) compare to the PFO kinetic equation. Additionally, the calculated adsorption data ($q_{e,\,cal}$) for PSO and the experimental value ($q_{e,\,exp}$) are also close.

The experimental results fit the PSO equation ($R^2 > 0.99$) more closely than the PFO kinetic equation. In addition, the calculated adsorption capacity ($q_{e,\,cal}$) is also comparable to the experimental value for PSO ($q_{e,\,exp}$). Therefore, the adsorption kinetics better fitted with the PSO model, suggesting the chemisorption mechanism of Cd^{2+}, Pb^{2+}, and Cr^{3+} ions adsorption [8].

3.2.7. Thermodynamics Studies of Metal Ions Adsorption. The impact of temperature of Cd^{2+}, Pb^{2+}, and Cr^{3+} ions adsorption on adsorbent was investigated at three different temperatures varied from 25 to 45°C. Figure 12 shows that the adsorption capacity for all metal ions was slightly increased as the temperature rose.

Various thermodynamic properties, such as free energy (ΔG), enthalpy (ΔH), and entropy change (ΔS), were calculated using the following Equations (10)–(12).

$$\Delta G = -\mathrm{RT} \ln K_d, \tag{10}$$

$$\Delta G = \Delta H - T\Delta S, \tag{11}$$

$$\ln K_d = \frac{\Delta \mathrm{S}}{R} - \frac{\Delta \mathrm{H}}{RT}, \tag{12}$$

where ΔH (kJ mol^{-1}) stands for change in enthalpy, G (kJ mol^{-1}) is for change in Gibbs free energy, and S (Jk^{1} mol^{-1} K^{-1}) is for change in entropy. R is gas constant

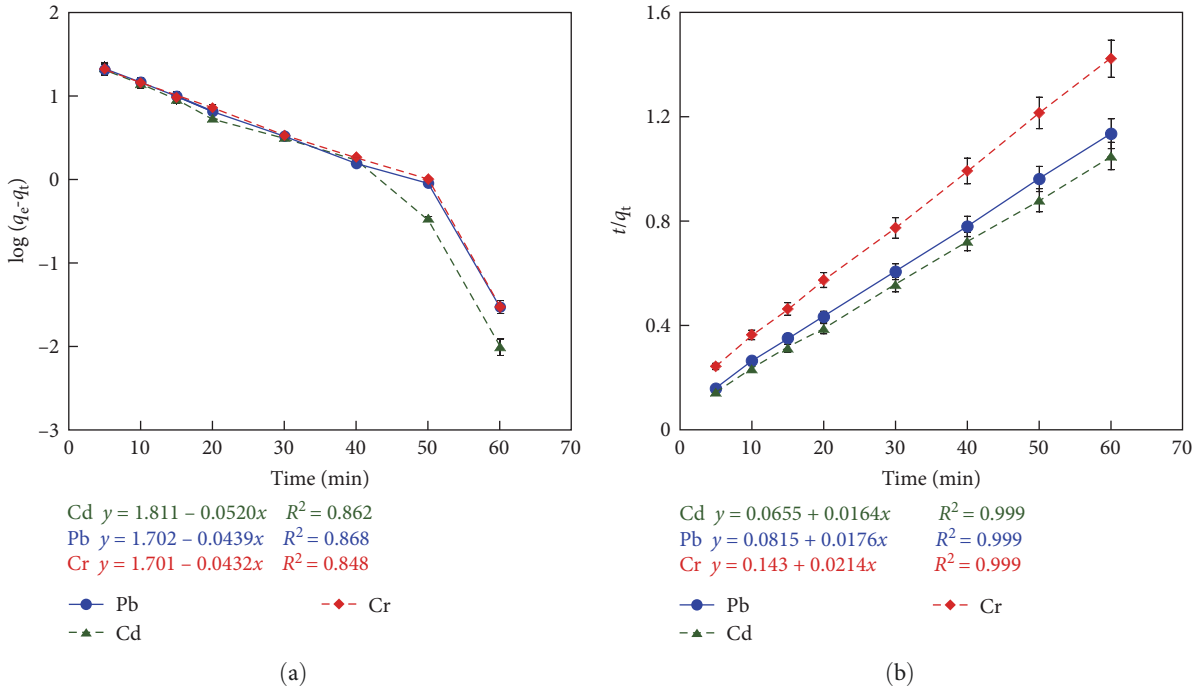

FIGURE 11: Kinetic plots of metal ions adsorption (a) pseudo-first-order and (b) pseudo-second-order ($T = 298$ K; $t = 60$ min; dosage = 1 g L^{-1}, metal ion concentraion = 60 ppm, and pH = 6).

TABLE 4: Kinetic data for adsorption of Cd^{2+}, Pb^{2+}, and Cr^{3+} onto the composite adsorbent.

Metal ions	Pseudo-first-order				Pseudo-second-order		
	$q_{e,\,exp}$	k_1	$q_{e,\,cal}$	R^2	k_2	$q_{e,\,cal}$	R^2
Cd^{2+}	57.03	0.1145	64.729	0.862	0.0041	60.98	0.999
Pb^{2+}	52.77	0.0967	50.304	0.868	0.0038	56.82	0.999
Cr^{3+}	42.09	0.0950	50.198	0.848	0.0032	46.73	0.999

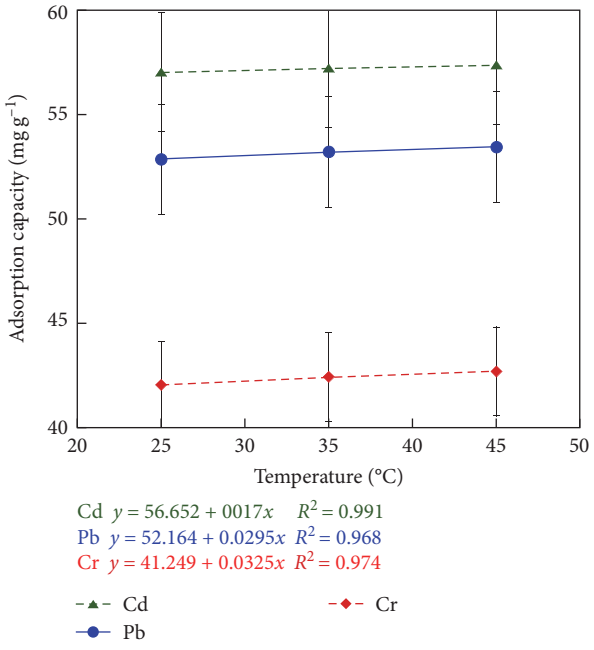

FIGURE 12: Adsorption capacity variation with temperature ($T = 298$ K; $t = 60$ min; dosage = 1 g L^{-1}, metal concentration = 60 ppm, and pH = 6).

(8.314 J mol^{-1} K^{-1}), T is the temperature in Kelvin, and K_d is the distribution coefficient of the adsorption process. The distribution coefficient was calculated using the following Equation (13).

$$K_d = \frac{q_e}{C_e}, \tag{13}$$

where q_e (mg L^{-1}) and C_e (mg L^{-1}) are metal ions concentration on the adsorbent and in the liquid phase at equilibrium. The values of ΔH and ΔS were obtained from the plot between ln K_d versus $1/T$ as shown in Figure 13, and the value of ΔG was computed from Equation (10).

Thermodynamic parameter values are summarized in Table 5. The positive ΔH values indicate that Cd^{2+}, Pb^{2+}, and Cr^{3+} ions adsorption reactions on composite adsorbent were endothermic, and adsorption was increased with rising temperature [41]. Furthermore, the positive value suggests that the chemisorption mechanism mainly controlled the removal of Cd^{2+}, Pb^{2+}, and Cr^{3+} from the aqueous solution [42]. Entropy values for all metal ions are positive, suggesting more unpredictability at the solid–liquid interface throughout

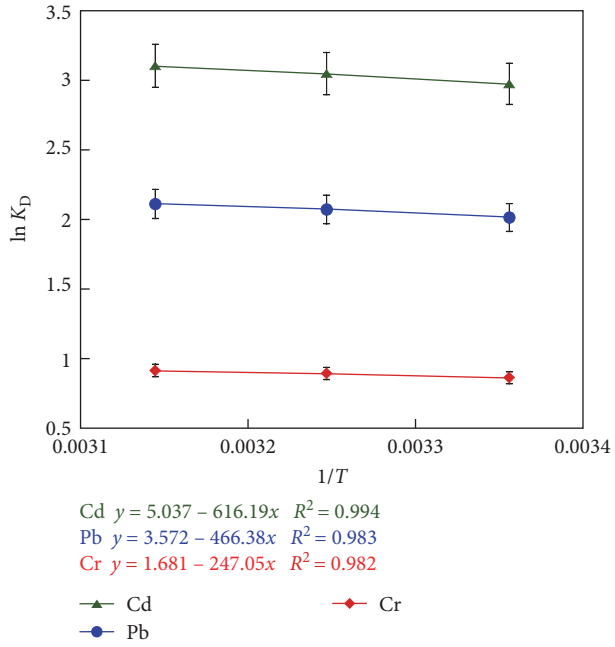

FIGURE 13: Thermodynamic of metal ions adsorption ($T = 298$ K; $t = 60$ min; dosage = 1 g L^{-1}, metal concentration = 60 ppm, and pH = 6).

TABLE 5: Thermodynamic properties of Cd^{2+}, Pb^{2+}, and Cr^{3+} adsorption onto composite adsorbent.

Metal ions	T (K)	q_{exp} (mg g^{-1})	ΔG (kJ mol^{-1})	ΔH (kJ mol^{-1})	ΔS (JK^{-1} mol^{-1})
Cd^{2+}	298	57.07	−7.353	5.123	41.882
	308	57.26	−7.788		
	318	57.41	−8.190		
Pb^{2+}	298	52.88	−4.967	3.877	29.701
	308	53.24	−5.284		
	318	53.47	−5.560		
Cr^{3+}	298	42.04	−2.108	2.054	13.977
	308	42.43	−2.258		
	318	42.69	−2.387		

the adsorption process. In addition, these metal ions had a higher affinity for the composite adsorbent [43]. Furthermore, the Gibbs free energy change values G for Cd^{2+}, Pb^{2+}, and Cr^{3+} varied from −7.353 to −8.190 kJ mol^{-1}, −4.967 to −5.560 kJ mol^{-1}, and −2.108 to −2.387 kJ mol^{-1}, respectively. These negative values at the studied temperature showed the applicability and spontaneity of the sorption process [44].

3.2.8. Competitive Adsorption. Gelatin blended composite adsorbent showed the metal ions adsorption under the ternary system of Cd^{2+}, Pb^{2+}, and Cr^{3+} with the metal removal percentage as 95%, 88%, and 70%, respectively. The studied metal ion's adsorption capacity by other adsorbents compared with this study is shown in Table 6.

3.2.9. Error Function. Data samples from each experiment in a series differ due to measurement errors that affect data accuracy. The statistical error function is assessed to correct the data errors for reliable results [11]. As a result, five error functions were used to examine the isotherm and kinetic data in order to assess the models' suitability. Higher values of r^2 and lower values of HYBRID, MPSD, χ^2, RMSE, and EABS, signify the model's best fit, respectively.

The correlation of regression (r^2) for the adsorption isotherm models suggests that Cd^{2+}, Pb^{2+}, and Cr^{3+} follow the Langmuir model. The error functions of the isotherm data (Table 7) suggest that D–R model provides the best fit for the experimental data. However, its regression co-efficient value are much lower therefore, cannot accept. Again, the correlation of regression (r^2) and the error functions for the kinetic models (Table 8) shows that PSO is the best-fit model. It is, therefore, strongly suggested from the regression coefficient (r^2) and error function that Langmuir model and PSO were the best-fit model of the studied adsorption.

Table 6: Comparative studied of maximum adsorption capacity of ternary metals ions by other adsorbents.

Adsorbent	Metal ions	Maximum adsorption capacity (mg g^{-1})	References
Synthesized silicate porous material (SPM)	Pb^{2+}	44.83	[45]
	Cd^{2+}	35.36	
Sultone-modified magnetic activated carbon bioadsorbent	Pb^{2+}	147.05	[46]
	Cd^{2+}	119.04	
Chitosan blended modified cellulose	Cr^{3+}	55	[15]
	Pb^{2+}	80	
	Cd^{2+}	91	
β-Cyclodextrin polymers	Pb^{2+}	196.4	[47]
	Cd^{2+}	136.4	
Carboxyl functionalized biosorbent	Pb^{2+}	49.86	[48]
	Cd^{2+}	49.44	
	Cr^{3+}	47.98	
Chitosan-pyromellitic dianhydride modified biochar	Pb^{2+}	8.263	[49]
	Cd^{2+}	24.677	
	Cu^{2+}	66.743	
Groundnut shell	Pb^{2+}	3.53	[50]
Gelatin blended modified cellulose	Cd^{2+}	101.420	This study
	Pb^{2+}	85.485	
	Cr^{3+}	72.213	

Table 7: Isotherm models error analysis data.

Metal ions	Isotherm model	Error function				EABS
		HYBRID	MPSD	χ^2	RMSE	
Cd^{2+}	Langmuir	8.715	3.909	0.464	7.050	7.050
	Freundlich	6.908	3.618	0.366	6.038	6.038
	Temkin	4.520	3.280	0.238	4.358	9.496
	D–R	108.961	104.384	6.972	24.928	24.928
Pb^{2+}	Langmuir	75.437	86.855	4.651	19.952	19.952
	Freundlich	29.079	53.925	1.674	11.054	11.054
	Temkin	7.404	27.210	0.393	6.498	6.498
	D–R	6.605	25.701	0.350	5.904	5.904
Cr^{3+}	Langmuir	2.629	16.216	0.137	3.324	3.324
	Freundlich	0.187	4.330	0.009	1.034	1.034
	Temkin	1.291	11.362	0.063	2.610	2.610
	D–R	1.343	1.343	0.069	2.376	2.376

Table 8: Kinetic models error analysis data.

Metal ions	Kinetic model	Error function				EABS
		HYBRID	MPSD	χ^2	RMSE	
Cd^{2+}	1st order	41.574	0.416	1.831	15.398	15.398
	2nd order	10.943	0.109	0.512	7.900	7.900
Pb^{2+}	1st order	4.610	0.046	0.242	4.932	4.932
	2nd order	12.433	0.124	0.577	8.100	8.100
Cr^{3+}	1st order	63.665	0.637	2.665	16.356	16.356
	2nd order	21.118	0.211	0.949	9.420	9.420

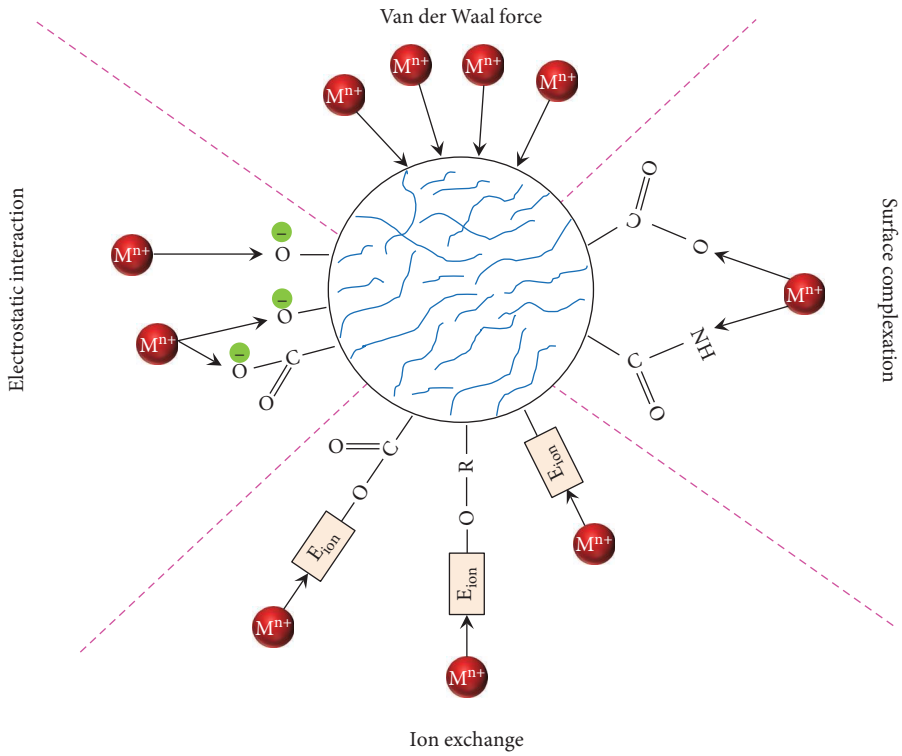

FIGURE 14: Schematic illustration of metal ions adsorption mechanism.

4. Mechanism of Metal Ions Adsorption

The composite adsorbent containing *N*, *O*, and *C* elements was confirmed by EDX analysis. FTIR spectra showed that composite adsorbent contained gelatin and α-cellulosic functional groups. Moreover, oxalic acid was used during adsorbent synthesis, probably including the acid functional groups in the adsorbent. Consequently, the adsorbent has several functional groups, such as acidic (–COOH), hydroxyl (–OH), amide linkage ($–CONH_2$), and so forth. Moreover, some mesopores or macropores were present on the adsorbent surface due to the acidic oxidation or mechanical friction that severely damaged the surface micropores of the adsorbent. Consequently, the possible metal ions adsorption mechanism may be explained: (i) the complexion with various functional groups can trap metal ions [51], (ii) Van der Waals force that bind the metal ions on adsorbent surface [52], (iii) ion-exchange process, the carboxylic group and the amide group ($–CONH_2–$) exchange cations (H^+) with metal ions [53] and, (iv) electrostatic interaction between metal ions and opposite charge of the adsorbent [18]. Figure 14 illustrates the metal ions adsorption onto composite adsorbent. Chemisorption process mainly controls the metal ions adsorption due to the 2nd order reaction kinetic.

5. Cost Analysis of Adsorbent for Cd^{2+}, Pb^{2+}, and Cr^{3+} Adsorption

The composite adsorbent was synthesized using very few chemicals. All basic raw materials are easily available, environment-friendly, and low cost. The cost was estimated based on adsorbent cost, processing charges, pH adjustment, batch operation, and adsorbate loading [50, 54]. The total cost with each parameter costing is given below.

5.1. Adsorbent Cost. Jute fiber is easily available in Bangladesh and its price is also very low compared to other adsorbent materials. The gelatin price is also cheap. Therefore, the average cost per gram of adsorbent was around 0.00054 $ from the local market.

5.2. Processing Charges. Low cost and fewer amounts of chemicals were required for synthesizing of composite adsorbent. After processing, the adsorbent were dried for short time, therefore, electricity bill was also low. According to chemicals and electricity used, it has been estimated cost 0.00084 $ per gram of adsorbent.

5.3. pH Adjustment. The metal ions adsorption was varied with changing solution pH. The optimum pH was 6 for the experiments. For this adjustment, hydrochloric acid (HCl) was used to adjust the solution pH, which costs almost 0.0001 $ per gram of adsorbent.

5.4. Batch Operation. The batch mode of operation required continuous stirring and operation time was 180 min, very small amount of electrical energy was required to conduct the experiments. The cost was almost 0.00051 $ per gram of metal ions adsorption.

5.5. Adsorbate Loading. It depends upon nature of the metal ions and adsorption capacity. The composite adsorbent showed adsorption capacity of 101.420, 85.485, and 72.213 $mg\,g^{-1}$ for Cd^{2+}, Pb^{2+}, and Cr^{3+} metal ions, respectively.

5.6. Cost Per Gram of Metal Ions Adsorption. The cumulative metal ions adsorption per g of adsorbent was 259.118 mg. Therefore, 1 g of metal ions adsorption required 3.861 g adsorbent. The following calculation gives the total cost per average gram of metal ions adsorption.

$$\begin{aligned}\text{Total cost} &= (0.00054 \times 3.861) + (0.00084 \times 3.861) \\ &\quad + (0.0001 \times 3.861) + 0.00051 \\ &= 0.00622\$\,\text{g}^{-1} \text{ of metal ions.}\end{aligned} \tag{14}$$

6. Conclusion

This study demonstrates the potential of using a biodegradable composite of gelatin and modified cellulose as an effective adsorbent for the simultaneous removal of Cd^{2+}, Pb^{2+}, and Cr^{3+} ions from aqueous solutions. The composite adsorbent was synthesized by a simple and easy method and showed high adsorption capacity and selectivity for the metal ions. Adsorption followed the Langmuir isotherm model and PSO kinetics, suggesting monolayer adsorption of metal ions onto homogeneous surfaces and a chemisorption mechanism. Adsorption was spontaneous and thermodynamically favorable. Maximum removal of 95%, 88%, and 70% for Cd^{2+}, Pb^{2+}, and Cr^{3+} ions was achieved in the batch experiment at pH 6 and metal ions concentration of 60 ppm. Therefore, composite adsorbent can be used as an environmental-friendly and cost-effective alternative to conventional adsorbents for the treatment of industrial wastewater containing heavy metal ions.

One of the limitations of this study is that the adsorption experiments were conducted using synthetic solutions containing Cd^{2+}, Pb^{2+}, and Cr^{3+} ions. The performance of the adsorbent may vary in real industrial effluent due to the presence of other contaminants, complex matrices, and interfering substances. Therefore, future studies should test the applicability of the adsorbent in real wastewater samples and compare the results with those obtained from synthetic solutions. This will provide more insights into the feasibility and practicality of the adsorbent for industrial wastewater treatment. MCC adsorbent has some advantages such as biodegradability, eco-friendliness, and high adsorption capacity. However, the stability of the adsorbent may depend on various factors such as the synthesis method, the drying mode, the content of MCC and the type of pollutants. Therefore, more studies are needed to verify the stability of the prepared MCC adsorbent under different conditions and applications.

Data Availability

All data generated through the experiments and analyzed during this study are included in this article.

Conflicts of Interest

The authors declare that they have no conflicts of interest.

Authors' Contributions

Marzia Sultana: conceptualization, data curation, investigation, visualization, and writing–original draft. Md. Raju Ahmmed: data curation, investigation, visualization, and writing–original draft. Md Inzamam Ul Hoque: data curation, investigation, visualization, and writing–original draft. Tanvir Ebna Mohsen: data curation, investigation, and formal analysis. Atol Mondal: data curation, investigation, and formal analysis. Md. Hafezur Rahaman: methodology, resources, writing–review and editing. Moumita Yesmin: data curation and investigation. Md. Shahedur Rahman: formal analysis, and writing–review and editing. S. M. Nur Alam: conceptualization, data curation, formal analysis, funding acquisition, methodology, project administration, resources, Ssupervision, validation, visualization, writing–original draft, and writing–review and editing.

Acknowledgments

This research work was partly supported by University Grants Commission (UGC, Bangladesh) memo no. 37.01.0000.073.06.052.22.1093.

References

[1] J. Li, X. Wang, G. Zhao et al., "Metal–organic framework-based materials: superior adsorbents for the capture of toxic and radioactive metal ions," *Chemical Society Reviews*, vol. 47, no. 7, pp. 2322–2356, 2018.

[2] S. Mishra, R. N. Bharagava, N. More et al., "Heavy metal contamination: an alarming threat to environment and human health," in *Environmental Biotechnology: For Sustainable Future*, R. Sobti, N. Arora, and R. Kothari, Eds., pp. 103–125, Springer, Singapore, 2019.

[3] G. Pooja, P. Senthil Kumar, G. Prasannamedha, S. Varjani, and D.-V. N. Vo, "Sustainable approach on removal of toxic metals from electroplating industrial wastewater using dissolved air flotation," *Journal of Environmental Management*, vol. 295, Article ID 113147, 2021.

[4] J. Xu, Z. Cao, Y. Zhang et al., "A review of functionalized carbon nanotubes and graphene for heavy metal adsorption from water: preparation, application, and mechanism," *Chemosphere*, vol. 195, pp. 351–364, 2018.

[5] A. Nargis, A. Habib, Harun-Or-Rashid et al., "Status of multielement in water of the river Buriganga, Bangladesh: aquatic chemistry of metal ions in polluted river water," *Emerging Contaminants*, vol. 7, pp. 99–115, 2021.

[6] W.-S. Zhong, T. Ren, and L.-J. Zhao, "Determination of Pb (Lead), Cd (Cadmium), Cr (Chromium), Cu (Copper), and Ni (Nickel) in Chinese tea with high-resolution continuum source graphite furnace atomic absorption spectrometry," *Journal of Food and Drug Analysis*, vol. 24, no. 1, pp. 46–55, 2016.

[7] M. T. Hossain, S. Khandaker, M. M. Bashar et al., "Simultaneous toxic Cd(II) and Pb(II) encapsulation from contaminated water using Mg/Al-LDH composite materials," *Journal of Molecular Liquids*, vol. 368, Part B, Article ID 120810, 2022.

[8] G. F. Coelho, A. C. Gonçalves Jr., D. Schwantes et al., "Removal of Cd(II), Pb(II) and Cr(III) from water using modified residues of *Anacardium occidentale* L." *Applied Water Science*, vol. 8, Article ID 96, 2018.

[9] M. Sultana, M. H. Rownok, M. Sabrin, M. H. Rahaman, and S. M. Nur Alam, "A review on experimental chemically modified activated carbon to enhance dye and heavy metals adsorption," *Cleaner Engineering and Technology*, vol. 6, Article ID 100382, 2022.

[10] J. Kamcev, D. R. Paul, and B. D. Freeman, "Ion activity coefficients in ion exchange polymers: applicability of manning's counterion condensation theory," *Macromolecules*, vol. 48, no. 21, pp. 8011–8024, 2015.

[11] M. S. Rahman and K. V. Sathasivam, "Heavy metal adsorption onto *Kappaphycus* sp. from aqueous solutions: the use of error functions for validation of isotherm and kinetics models," *BioMed Research International*, vol. 2015, Article ID 126298, 13 pages, 2015.

[12] Q. Chen, Y. Yao, X. Li, J. Lu, J. Zhou, and Z. Huang, "Comparison of heavy metal removals from aqueous solutions by chemical precipitation and characteristics of precipitates," *Journal of Water Process Engineering*, vol. 26, pp. 289–300, 2018.

[13] F. Almomani, R. Bhosale, M. Khraisheh, A. Kumar, and T. Almomani, "Heavy metal ions removal from industrial wastewater using magnetic nanoparticles (MNP)," *Applied Surface Science*, vol. 506, Article ID 144924, 2020.

[14] W. S. Chai, J. Y. Cheun, P. Senthil Kumar et al., "A review on conventional and novel materials towards heavy metal adsorption in wastewater treatment application," *Journal of Cleaner Production*, vol. 296, Article ID 126589, 2021.

[15] M. H. Rahaman, M. A. Islam, M. M. Islam, M. A. Rahman, and S. M. Nur Alam, "Biodegradable composite adsorbent of modified cellulose and chitosan to remove heavy metal ions from aqueous solution," *Current Research in Green and Sustainable Chemistry*, vol. 4, Article ID 100119, 2021.

[16] X.-J. Li, W.-R. Cui, W. Jiang, R.-H. Yan, R.-P. Liang, and J.-D. Qiu, "Bi-functional natural polymers for highly efficient adsorption and reduction of gold," *Chemical Engineering Journal*, vol. 422, Article ID 130577, 2021.

[17] A. Guleria, G. Kumari, E. C. Lima, D. K. Ashish, V. Thakur, and K. Singh, "Removal of inorganic toxic contaminants from wastewater using sustainable biomass: a review," *Science of The Total Environment*, vol. 823, Article ID 153689, 2022.

[18] N. A. Fakhre and B. M. Ibrahim, "The use of new chemically modified cellulose for heavy metal ion adsorption," *Journal of Hazardous Materials*, vol. 343, pp. 324–331, 2018.

[19] S. Pahoff, C. Meinert, O. Bas, L. Nguyen, T. J. Klein, and D. W. Hutmacher, "Effect of gelatin source and photoinitiator type on chondrocyte redifferentiation in gelatin methacryloyl-based tissue-engineered cartilage constructs," *Journal of Materials Chemistry B*, vol. 7, no. 10, pp. 1761–1772, 2019.

[20] K. Lerdchai, J. Kitsongsermthon, J. Ratanavaraporn, S. Kanokpanont, and S. Damrongsakkul, "Thai silk fibroin/gelatin sponges for the dual controlled release of curcumin and docosahexaenoic acid for anticancer treatment," *Journal of Pharmaceutical Sciences*, vol. 105, no. 1, pp. 221–230, 2015.

[21] J. Alipal, N. A. S. Mohd Pu'ad, T. C. Lee et al., "A review of gelatin: properties, sources, process, applications, and commercialisation," *Materials Today: Proceedings*, vol. 42, Part 1, pp. 240–250, 2021.

[22] M. H. Rahaman, M. M. Rana, M. A. Gafur, and A. A. Mohona, "Preparation and analysis of poly(*l*-lactic acid) composites with oligo(*d*-lactic acid)-grafted cellulose," *Journal of Applied Polymer Science*, vol. 136, no. 18, Article ID 47424, 2019.

[23] J. Uranga, A. I. Puertas, A. Etxabide, M. T. Dueñas, P. Guerrero, and K. de la Caba, "Citric acid-incorporated fish gelatin/chitosan composite films," *Food Hydrocolloids*, vol. 86, pp. 95–103, 2019.

[24] L. Sun, J. Wang, J. Wu et al., "Constructing nanostructured silicates on diatomite for Pb(II) and Cd(II) removal," *Journal of Materials Science*, vol. 54, pp. 6882–6894, 2019.

[25] A. Hashem, S. M. Badawy, S. Farag, L. A. Mohamed, A. J. Fletcher, and G. M. Taha, "Non-linear adsorption characteristics of modified pine wood sawdust optimised for adsorption of Cd(II) from aqueous systems," *Journal of Environmental Chemical Engineering*, vol. 8, no. 4, Article ID 103966, 2020.

[26] S. Karakuş, N. Taşaltın, C. Taşaltın, and A. Kilislioğlu, "Comparative study on ultrasonic assisted adsorption of Basic Blue 3, Basic Yellow 28 and Acid Red 336 dyes onto hydromagnesite stromatolite: kinetic, isotherm and error analysis," *Surfaces and Interfaces*, vol. 20, Article ID 100528, 2020.

[27] F. Batool, J. Akbar, S. Iqbal, S. Noreen, and S. N. A. Bukhari, "Study of isothermal, kinetic, and thermodynamic parameters for adsorption of cadmium: an overview of linear and nonlinear approach and error analysis," *Bioinorganic Chemistry and Applications*, vol. 2018, Article ID 3463724, 11 pages, 2018.

[28] G. Vilardi, L. Di Palma, and N. Verdone, "Heavy metals adsorption by banana peels micro-powder: equilibrium modeling by non-linear models," *Chinese Journal of Chemical Engineering*, vol. 26, no. 3, pp. 455–464, 2018.

[29] H. Rahaman, S. Hosen, A. Gafur, and R. Habib, "Small amounts of poly(*D*-lactic acid) on the properties of poly(*L*-lactic acid)/microcrystalline cellulose/poly(*D*-lactic acid) blends," *Results in Materials*, vol. 8, Article ID 100125, 2020.

[30] R. Md Salim, J. Asik, and M. S. Sarjadi, "Chemical functional groups of extractives, cellulose and lignin extracted from native *Leucaena leucocephala* bark," *Wood Science and Technology*, vol. 55, pp. 295–313, 2021.

[31] Y. Pei, D. Ye, Q. Zhao et al., "Effectively promoting wound healing with cellulose/gelatin sponges constructed directly from a cellulose solution," *Journal of Materials Chemistry B*, vol. 3, no. 38, pp. 7518–7528, 2015.

[32] İ. Sargın and G. Arslan, "Chitosan/sporopollenin microcapsules: preparation, characterisation and application in heavy metal removal," *International Journal of Biological Macromolecules*, vol. 75, pp. 230–238, 2015.

[33] L. Pan, P. Li, and Y. Tao, "Preparation and properties of microcrystalline cellulose/fish gelatin composite film," *Materials*, vol. 13, no. 19, Article ID 4370, 2020.

[34] E. Igberase, A. Ofomaja, and P. O. Osifo, "Enhanced heavy metal ions adsorption by 4-aminobenzoic acid grafted on chitosan/epichlorohydrin composite: kinetics, isotherms, thermodynamics and desorption studies," *International Journal of Biological Macromolecules*, vol. 123, pp. 664–676, 2019.

[35] J. Qiu, S. Dong, H. Wang, X. Cheng, and Z. Du, "Adsorption performance of low-cost gelatin–montmorillonite nanocomposite for Cr(iii) ions," *RSC Advances*, vol. 5, no. 72, pp. 58284–58291, 2015.

[36] M. Mahmood-ul-Hassan, M. Yasin, M. Yousra, R. Ahmad, and S. Sarwar, "Kinetics, isotherms, and thermodynamic studies of lead, chromium, and cadmium bio-adsorption from aqueous solution onto *Picea smithiana* sawdust," *Environmental Science and Pollution Research*, vol. 25, pp. 12570–12578, 2018.

[37] A. A. Taha, M. A. Shreadah, A. M. Ahmed, and H. F. Heiba, "Multi-component adsorption of Pb(II), Cd(II), and Ni(II) onto Egyptian Na-activated bentonite; equilibrium, kinetics, thermodynamics, and application for seawater desalination," *Journal of Environmental Chemical Engineering*, vol. 4, no. 1, pp. 1166–1180, 2016.

[38] M. S. Masoud, A. A. Zidan, G. M. El Zokm, R. M. I. Elsamra, and M. A. Okbah, "Humic acid and nano-zeolite NaX as low

cost and eco-friendly adsorbents for removal of Pb(II) and Cd (II) from water: characterization, kinetics, isotherms and thermodynamic studies," *Biomass Conversion and Biorefinery*, 2022.

[39] N. Can, B. C. Ömür, and A. Altındal, "Modeling of heavy metal ion adsorption isotherms onto metallophthalocyanine film," *Sensors and Actuators B: Chemical*, vol. 237, pp. 953–961, 2016.

[40] G. M. Al-Senani and F. F. Al-Fawzan, "Adsorption study of heavy metal ions from aqueous solution by nanoparticle of wild herbs," *The Egyptian Journal of Aquatic Research*, vol. 44, no. 3, pp. 187–194, 2018.

[41] S. Guo, P. Jiao, Z. Dan et al., "Synthesis of magnetic bioadsorbent for adsorption of Zn(II), Cd(II) and Pb(II) ions from aqueous solution," *Chemical Engineering Research and Design*, vol. 126, pp. 217–231, 2017.

[42] Y. Jia, Y. Zhang, J. Fu et al., "A novel magnetic biochar/MgFe-layered double hydroxides composite removing Pb^{2+} from aqueous solution: Isotherms, kinetics and thermodynamics," *Colloids and Surfaces A: Physicochemical and Engineering Aspects*, vol. 567, pp. 278–287, 2019.

[43] L. Cui, Y. Wang, L. Gao et al., "EDTA functionalized magnetic graphene oxide for removal of Pb(II), Hg(II) and Cu(II) in water treatment: adsorption mechanism and separation property," *Chemical Engineering Journal*, vol. 281, pp. 1–10, 2015.

[44] X. Zhou, J. Zhou, Y. Liu, J. Guo, J. Ren, and F. Zhou, "Preparation of iminodiacetic acid-modified magnetic biochar by carbonization, magnetization and functional modification for Cd(II) removal in water," *Fuel*, vol. 233, pp. 469–479, 2018.

[45] D. Ouyang, Y. Zhuo, L. Hu, Q. Zeng, Y. Hu, and Z. He, "Research on the adsorption behavior of heavy metal ions by porous material prepared with silicate tailings," *Minerals*, vol. 9, no. 5, Article ID 291, 2019.

[46] V. Nejadshafiee and M. R. Islami, "Adsorption capacity of heavy metal ions using sultone-modified magnetic activated carbon as a bio-adsorbent," *Materials Science and Engineering: C*, vol. 101, pp. 42–52, 2019.

[47] J. He, Y. Li, C. Wang et al., "Rapid adsorption of Pb, Cu and Cd from aqueous solutions by β-cyclodextrin polymers," *Applied Surface Science*, vol. 426, pp. 29–39, 2017.

[48] S. Mahour, S. K. Verma, J. K. Arora, and S. Srivastava, "Carboxyl appended polymerized seed composite with controlled structural properties for enhanced heavy metal capture," *Separation and Purification Technology*, vol. 284, Article ID 120247, 2022.

[49] J. Deng, Y. Liu, S. Liu et al., "Competitive adsorption of Pb(II), Cd(II) and Cu(II) onto chitosan-pyromellitic dianhydride modified biochar," *Journal of Colloid and Interface Science*, vol. 506, pp. 355–364, 2017.

[50] A. Das, N. Bar, and S. K. Das, "Adsorptive removal of Pb(II) ion on *Arachis hypogaea's* shell: batch experiments, statistical, and GA modeling," *International Journal of Environmental Science and Technology*, vol. 20, pp. 537–550, 2023.

[51] S. Xu, W. Yu, S. Liu, C. Xu, J. Li, and Y. Zhang, "Adsorption of hexavalent chromium using banana pseudostem biochar and its mechanism," *Sustainability*, vol. 10, no. 11, Article ID 4250, 2018.

[52] W. Kong, Q. Li, X. Li et al., "Removal of copper ions from aqueous solutions by adsorption onto wheat straw cellulose-based polymeric composites," *Journal of Applied Polymer Science*, vol. 135, no. 36, Article ID 46680, 2018.

[53] R. Wang, R. Liang, T. Dai, J. Chen, X. Shuai, and C. Liu, "Pectin-based adsorbents for heavy metal ions: a review," *Trends in Food Science & Technology*, vol. 91, pp. 319–329, 2019.

[54] S. Bhattacharya, N. Bar, B. Rajbansi, and S. K. Das, "Synthesis of chitosan-*n*TiO_2 nanocomposite, application in adsorptive removal of Cu(II)—adsorption and desorption study, mechanism, scale-up design, statistical, and genetic algorithm modeling," *Applied Organometallic Chemistry*, vol. 37, no. 6, Article ID e7094, 2023.